PERGAMON

International Journal of Multiphase Flow 26 (2000) 1439–1455

International Journal of Multiphase Flow

www.elsevier.com/locate/ijmulflow

Countercurrent gas–liquid flow in inclined and vertical ducts — I: Flow patterns, pressure drop characteristics and flooding

A. Zapke[a], D.G. Kröger[b,*]

[a]*GEA Aircooled Systems (Pty) Ltd, P.O. Box 1427, Germiston, 1400, South Africa*
[b]*Department of Mechanical Engineering, University of Stellenbosch, Matieland, 7602, South Africa*

Received 8 December 1998; received in revised form 29 August 1999

Abstract

An experimental investigation into adiabatic gas–liquid counterflow in inclined and vertical rectangular ducts with a square-edged gas inlet is conducted. Water, methanol, propanol, air, argon, helium and hydrogen are used as working fluids. The duct height and width are varied from 50 to 150 mm and 10 to 20 mm respectively. At low gas flow rates the two-phase pressure gradient is gas Reynolds number related while it becomes dependent on the densimetric gas Froude number as the gas flow is increased. The hydraulic diameter is the length dimension required for the gas Reynolds number, while the duct height becomes the characteristic dimension in the Froude number. The flooding gas velocity is found to be strongly dependent on the duct height, the phase densities and duct inclination. © 2000 Elsevier Science Ltd. All rights reserved.

Keywords: Gas–liquid flow; Counterflow; Flow patterns; Pressure drop; Flooding; Inclined ducts; Vertical ducts

1. Introduction

During countercurrent flow in ducts or tubes when liquid drains downwards against the walls under the action of gravity and there is upward gas flow, a transition to partial or complete upward liquid flow occurs at sufficiently high gas flow rates. Flooding forms part of this transition. The flooding phenomenon is encountered under a variety of conditions in reflux

* Corresponding author.

PII: S0301-9322(99)00097-X

condensers, packed columns, heat pipes and certain nuclear reactor accident scenarios and has been the subject of numerous investigations in the past. The present paper discusses the findings of an experimental investigation of the effect of the fluid properties and the duct geometry and inclination on flooding. The flooding data is based on the definition originally published by Hewitt and Hall-Taylor (1970). The definition is briefly described in the next paragraph.

Consider the vertical tube shown in Fig. 1. Liquid is injected into the tube at a constant rate through a porous section and is extracted smoothly at the bottom. At low gas flow rates a falling film exists [Fig. 1(a)]. As the gas flow is gradually increased, a rate is reached where the film becomes more wavy and eventually liquid is carried upwards as shown in Fig. 1(b). Liquid is now transported above the injection point and a flow pattern exists where climbing and falling film flow are occurring simultaneously as depicted in Fig. 1(c) and (d). The transition from pure counterflow to simultaneous liquid up- and downflow [Fig. 1(b)] is defined as flooding while the steady-state conditions in Fig. 1(c) and (d) are referred to as partial liquid delivery. With a further increase in the gas flow rate the liquid flow below the injection point changes to climbing film flow [Fig. 1(e)] and eventually all the liquid is carried upwards [Fig. 1(f)].

Once flooding has occurred the liquid above the porous inlet does not necessarily proceed to leave the test section. In the case of low liquid flow rates it may form a hanging film above the porous inlet without a net upward flow, as described by Govan et al. (1991). At higher liquid flow rates flooding causes a direct transition from pure countercurrent flow to a state of partial liquid delivery, resulting in net upward flow of liquid (Clift et al., 1966; Suzuki and Ueda,

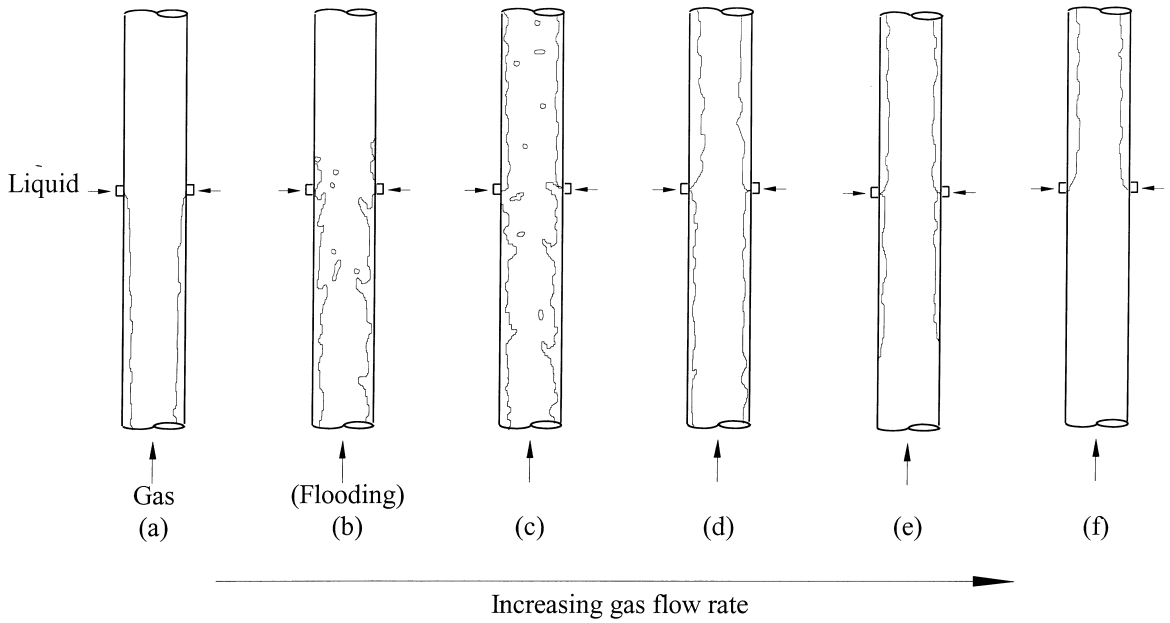

Fig. 1. Flow transitions from countercurrent flow to cocurrent upflow in vertical tubes.

1977; Govan et al., 1991). Consequently a marked decrease in the liquid downflow rate is experienced. Note that depending on the gas inlet geometry, some liquid may be carried above the porous section in the form of entrained droplets prior to the condition depicted in Fig. 1(b). This is not regarded as flooding (Whalley and McQuillan, 1985; Govan et al., 1991).

The effect of the liquid properties on flooding has been addressed by a number of researchers, e.g. Feind (1960), Clift et al. (1966), Suzuki and Ueda (1977) and Chung et al. (1980) to mention a few. More recently Zapke and Kröger (1996) published flooding results where the emphasis of the investigation was on the effect of both the gas and the liquid properties.

According to the experimental investigation by Feind (1960) about the pressure drop experienced by a gas during countercurrent gas–liquid flow, the interfacial shear is related to the gas Reynolds number in a manner similar to that of wall friction during single-phase flow. Flooding is however governed by the gas Froude number. Thus a transition from gas Reynolds number to gas Froude number governed dynamics appears to exist. It is the main aim of the present investigation to establish the role of these two dimensionless groups during countercurrent flow. This is achieved by conducting adiabatic experiments with different working fluids and duct geometries.

The effect of the duct inclination on flooding is addressed in detail. Little has been published so far on counterflow in inclined ducts compared to the extensive information available on two-phase flow in vertical tubes. Lee and Bankoff (1983, 1984) investigated steam-water counterflow in an inclined channel. The flooding steam velocity was the lowest for the smaller inclination angles and increased with an increase in inclination up to approximately 30°. For 31° and 87° the flooding steam velocities were approximately equal. The same trend was found by Barnea et al. (1986) who conducted air–water experiments in a 51 mm plexiglass tube.

2. Apparatus and experimental procedure

The configuration of inclined air-cooled reflux condensers was followed as a guide line to design an experimental apparatus. Such reflux condensers are employed as secondary condensers or dephlemators in the power industry where the turbine exhaust steam is condensed at sub-atmospheric pressures inside finned tubes. The finned tube profile can be round, elliptical or flattened. The lower ends of the finned tubes are welded into a tube sheet to form a square-edged vapour inlet. During total reflux condensation the phase velocities are the highest at this location. Flooding is therefore most likely to occur as a result of strong phase interaction at the square-edged gas or vapour inlet. For this reason a square-edged gas inlet was employed and the liquid inlet plenum was designed to prevent the introduction of flow disturbances at the liquid feed.

2.1. Flow loop

A schematic of the flow loop is shown in Fig. 2(a). The liquid flow, supplied by a constant head tank, is monitored by calibrated rotameters. It enters the duct through a porous section, drains downwards and subsequently enters the gas inlet plenum at the square-edged flange. A

pump circulates the liquid back to the constant head tank. Three standard orifice plates differing in size are employed to achieve the desired range of metered gas flow. The gas flows via an inlet plenum into the test section. The gas inlet plenum is constructed of a 0.72 m long and 0.286 m i.d. glass cylinder to enable visualisation of the draining liquid at the square-edged flange. A honeycomb section and a mesh are employed to dampen out local high velocities and to obtain a uniform velocity profile to the square-edged flange.

Water, methanol, propanol, air, helium, hydrogen and argon were used as working fluids. The exit of the test section was open to the atmosphere and hence the test pressure was just above the ambient pressure. The fluid temperature was close to the ambient temperature, i.e. $\approx 25^{\circ}C$. The fluid properties at the ambient conditions are given in Table 1.

The duct profiles tested are shown in Fig. 3(a). Fig. 3(b) illustrates a typical duct assembly. Two transparent acrylic plastic sheets bolted to grooved aluminium spacers form the duct walls. Three duct heights of 50, 100 and 150 mm and two widths of 10 and 20 mm were investigated.

2.2. Test section configuration for pressure drop measurements in inclined ducts

The change in static pressure across the square-edged flange was measured between P_1 and P_2 as indicated in Fig. 2(a), where the pressure tapping point P_1 is located inside the gas inlet

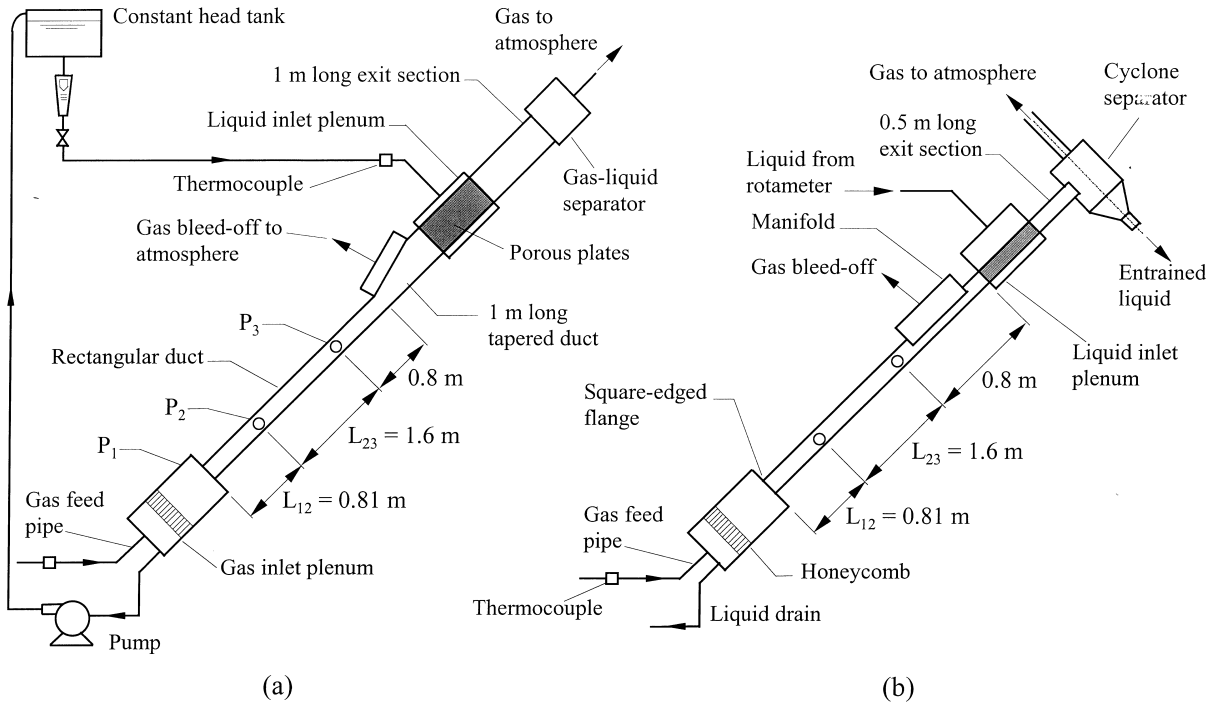

Fig. 2. (a) Schematic of the flow loop and test section configuration employed for pressure drop measurements in inclined ducts. (b) Test section configuration for flooding. No gas was bled off in the case of vertical flooding tests.

Table 1
Properties at ambient conditions ($p \approx 101{,}325$ N/m^2, $T \approx 295$ K) of the fluids that were used for the experimental investigation

Fluid	Density (kg/m^3)	Viscosity $\times 10^6$ (kg/ms)	Surface tension $\times 10^3$ (N/m)
Air	1.196	18.230	–
Argon	1.650	22.390	–
Helium	1.653×10^{-1}	20.040	–
Hydrogen	$8.325 \times {}^{-2}$	8.863	–
Water	998	958	72
Methanol	791	575	22
Isopropanol	784	2362	22

plenum and P_2 located at distance of 0.81 m above the square-edged flange. The pressure gradient experienced by the gas flow inside the duct in the presence of the draining liquid was obtained by measuring the pressure drop over a distance of 1.6 m between P_2 and P_3. The aim of these measurements was to generate pressure gradient data for counterflow in the absence of any flow disturbances introduced in the process of feeding liquid into the test section. For this purpose a tapered duct was inserted between the constant cross-sectional area test section and the porous inlet. The tapered duct acts as diffuser to slow down the gas velocity and thus prevents the liquid flow from being disturbed as it enters through the porous plates.

The porous section inside the liquid inlet plenum was constructed similarly to the duct depicted in Fig. 3(b), except that the acrylic plastic sheets were replaced by sintered bronze plates over a length of 260 mm. The inside height of the porous section was 185 mm. In the case of the 100 and 150 mm ducts the increased flow area at the porous plates proved to be insufficient to allow for the development of a smooth stratified liquid layer in the tapered

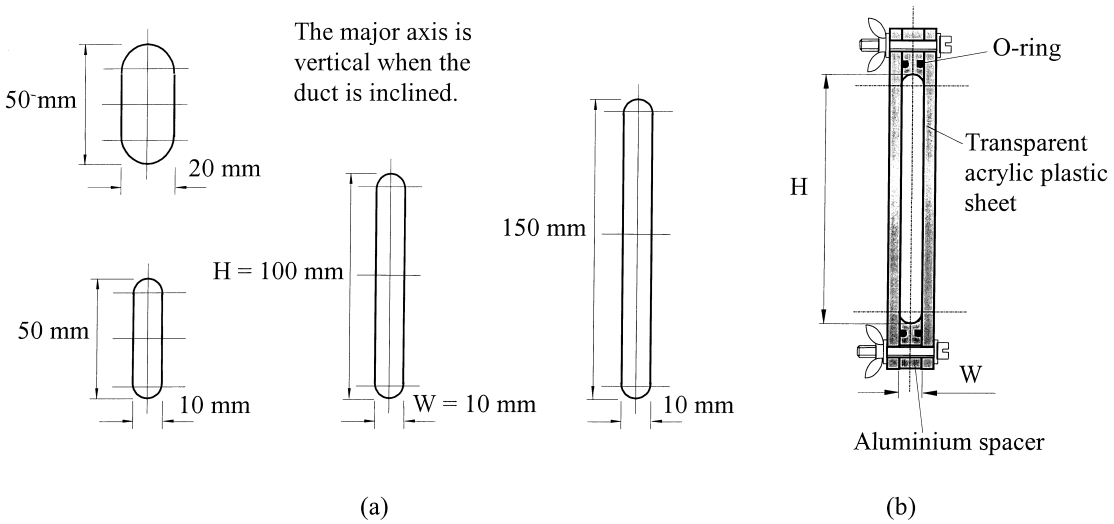

Fig. 3. (a) Duct profiles tested. (b) Cross-sectional view of the duct assembly.

section. Holes were therefore drilled into the acrylic plastic walls along the top of the tapered duct to allow part of the gas to escape before reaching the sintered plates.

During an experimental run the liquid flow was set at a predetermined rate while pressure drop measurements were conducted for various gas flow rates. The lowest gas flow rates tested correspond to a Reynolds number of approx. 500. The gas flow was allowed to stabilise, data were recorded and the gas flow rate was increased for the routine to be repeated, until flooding occurred. No data were recorded for conditions beyond flooding as those were beyond the scope of the investigation.

2.3. Test section configuration for flooding experiments in inclined and vertical ducts

The entire configuration illustrated in Fig. 2(a) is 7 m long and its maximum inclination is limited to $\approx 60^\circ$ to the horizontal by the laboratory roof. To conduct flooding experiments for inclinations from near horizontal to the vertical the apparatus was shortened by removing the tapered duct and mounting the 3.21 m long constant cross-sectional area test section directly onto the liquid inlet plenum as shown in Fig. 2(b). Holes were again drilled into the duct walls along the section between pressure tapping point 3 and the liquid inlet plenum to bleed-off part of the gas before reaching the porous plates. This ensured that flooding was caused by the gas–liquid interaction at the square-edged gas inlet, i.e. at the lower end of the duct.

Note that the flooding gas velocity was defined in the introduction as the gas flow rate at which liquid begins to be transported above the point of liquid injection. In the present apparatus upward transport of liquid broke down inside the zone of gas bleed-off and liquid was therefore not always propelled beyond the porous inlet. Flooding was hence defined as the conditions when liquid is propelled into the gas bleed-off zone. This may however not be regarded as a new or different definition because strictly speaking the "liquid feed" is located

Table 2
Summary of flooding experiments

Duct geometry	Duct inclination to the horizontal (°)	Fluid combination
$H = 50$ mm	2, 10, 20, 40, 60, 70, 80, 90	Air–water
$W = 10$ mm	2, 5, 10, 15, 20, 60, 80, 90	Air–propanol
	60, 90	Air–methanol
	60	Argon–water
	60	Helium–water
	60	Helium–methanol
	60	Hydrogen–methanol
$H = 100$ mm	2, 20, 40, 60, 70, 80, 90	Air–water
$W = 10$ mm	2, 40, 60, 90	Air–propanol
	60, 90	Air–methanol
$H = 150$ mm	2, 20, 40, 60, 90	Air–water
$W = 10$ mm	60, 90	Air–propanol
	60, 90	Air–methanol
$H = 50$ mm	2, 5, 10, 20, 40, 60, 70, 80, 90	Air–water
$W = 20$ mm		

just below the bleed-off zone where the full gas flow rate is still present inside the test section. Thus the transport of liquid into the bleed-off zone constitutes flooding because "liquid has been carried above the point of injection".

Exactly the same configuration was used for the flooding experiments for vertical counterflow except that no gas bleed-off was employed. In this case the test section configuration resembles the schematic depicted in Fig. 1 and the definition by Hewitt and Hall-Taylor (1970) could be followed to generate flooding data.

The fluid combinations, duct geometries and inclinations tested for flooding are summarised in Table 2.

3. Experimental results: flow patterns and pressure drop

Upon the onset of phase interaction at the square-edged gas inlet three types of flow patterns, depending on the duct inclination, were observed: (i) roll waves at inclinations close to the horizontal; (ii) a distinctive vortex-type flow at intermediate angles; and (iii) churn-type flow containing elements of the vortex flow in the case of vertical ducts.

3.1. Flow patterns observed at a duct inclination of 60° to the horizontal

At low gas flow rates there is no phase interaction and the liquid drains in the form of an undisturbed jet into the bottom plenum. Inside the test section the flow is stratified. There is no entrainment and the duct walls are dry. The pressure gradient and the entrance pressure drop are equal to the corresponding air-only values. As the gas flow rate is increased, the jet inside the plenum experiences an upward deflection as a result of the drag exerted by the gas flow. Droplets are entrained at the square-edged flange and deposited on the duct walls just above the inlet flange. The gas–liquid interface along the duct is fairly smooth but small waves travelling downwards are present. Upon a further increase in the air flow rate the jet of liquid inside the plenum is dispersed causing entrainment. Eventually an air flow rate is reached where the liquid jet is sporadically sucked into the test section.

The conditions where the draining liquid is sporadically sucked into the duct is the onset of a distinctive vortex-type flow at the square-edged flange. The vortex is formed as a result of simultaneous liquid up- and downflow when liquid draining downwards at the bottom of the duct is swept upwards by the gas flow, giving rise to the rotating action. Initially the rotational motion is confined to a small region just above the inlet flange at which time the vortex size or "diameter" is only a fraction of the duct height. As the gas flow rate is increased the vortex grows in size. Close to flooding the "diameter" approaches the duct height, as illustrated in Fig. 4. Just below the flooding gas velocity the rotating gas–liquid mixture constituting a vortex disintegrates after it has travelled ≈ 1 m up the duct. At flooding such a vortex travels all the way upwards to the gas bleed-off zone where it collapses. The flow becomes very transient in nature once vortices are present and very strong pressure pulses are generated in the process of vortex formation and disintegration.

3.2. Flow patterns observed in near horizontal and vertical ducts

At duct inclinations close to the horizontal the component of the gravity force which has to be overcome for the accumulation of liquid at the gas inlet and the subsequent upward transport thereof is relatively small. The gas velocity required to cause flooding is therefore significantly lower compared to steeper inclinations and consequently the phase interaction is less intensive. At sufficiently high gas flow rates roll waves formed at the bottom end of the test section are propelled upwards. They either disintegrate gradually or grow to bridge the duct height in which case the roll waves are propelled to the top end of the test section to cause flooding.

During counterflow in vertical ducts the flow is annular prior to the onset of strong phase interaction, instead of being stratified as in the case of inclined ducts. In the absence of gas flow the liquid drains in the form of a wavy film down the acrylic plastic walls. As the gas flow is increased the liquid starts to concentrate at the aluminium spacers, i.e. at the short sides of

Fig. 4. Air–water flow pattern inside the 100 mm duct inclined at 60° to the horizontal. $V_G = 19$ m/s, $V_L = 9.2 \times 10^{-3}$ m/s, $Re_G = 22300$, $Fr_{HG} = 0.41$.

the duct. At fairly low air velocities, approx. 3 m/s, liquid droplets are entrained at the square-edged flange. Initially these droplets are deposited onto the film in the immediate region above the inlet flange. At sufficiently high gas flow rates the droplets are carried beyond the liquid inlet sinter. The formation of a rough oscillating film at the square-edged flange follows the onset of entrainment. The liquid draining into the bottom plenum along the aluminium spacers is sporadically sucked into the test section resulting in intermittent penetration. As the gas flow rate is further increased this region of churn-type flow grows until it reaches the sinter inlet. Liquid is then transported above the sinter in the form of a churning flow and flooding occurs.

These observations are very similar to those by Govan et al. (1991) and Zapke and Kröger (1996) for vertical tubes with square-edged gas inlets, except that vortices could be observed in the rectangular ducts from time to time.

3.3. Pressure drop characteristics measured in ducts inclined at 60° to the horizontal

3.3.1. The effect of the duct geometry

In Fig. 5(a) the friction factor f_G as measured for air–water flow in the four ducts, is plotted against the superficial gas Reynolds number

$$Re_G = \frac{\rho_G V_G D_e}{\eta_G} \tag{1}$$

ρ_G and η_G are the gas density and viscosity respectively, V_G is the superficial gas velocity and D_e is the hydraulic diameter, f_G is the Darcy friction factor based on the superficial gas velocity, i.e.

$$f_G = (D_e/L_{23})\Delta p_{23}/(1/2\rho_G V_G^2) \tag{2}$$

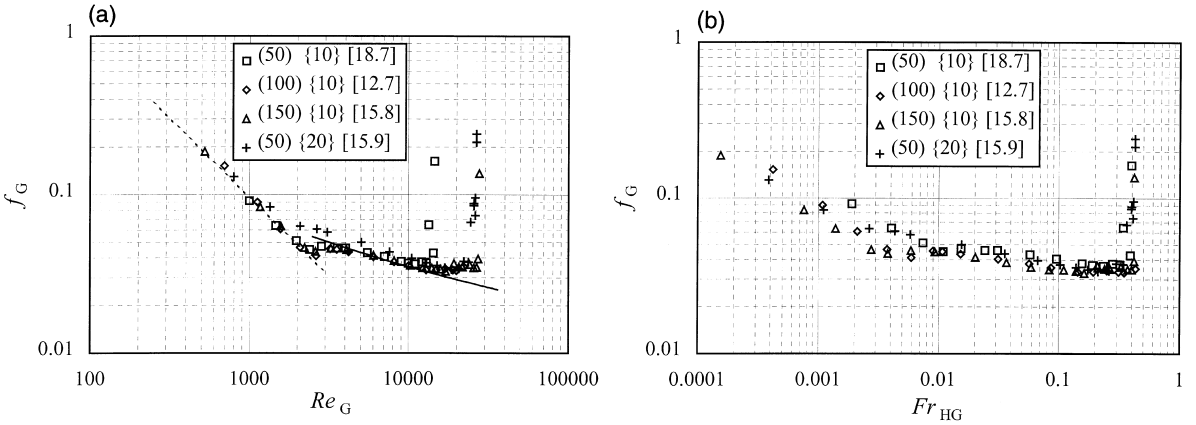

Fig. 5. (a) Air–water pressure drop measured for the four ducts inclined at 60°, presented in terms of a friction factor against the gas Reynolds number. (H), mm; $\{W\}$, mm; $[V_L]$, m/s × 10^3. Broken and solid line: Laminar and turbulent single-phase friction factor. (b) Air–water pressure drop measured for the four ducts inclined at 60°, presented in terms of a friction factor against the gas Froude number. (H), mm; $\{W\}$, mm; $[V_L]$, m/s × 10^3.

where Δp_{23} is the frictional pressure drop measured between P_2 and P_3, and L_{23} is the distance between P_2 and P_3. The broken line in Fig. 5(a) represents the friction factor for laminar single-phase flow between parallel plates

$$f = 96/Re \tag{3}$$

while the solid line is the turbulent friction factor for single-phase flow between parallel plates according to White (1991):

$$(1/f)^{1/2} = 2.0 \log_{10}\{Re(f)^{1/2}\} - 1.19 \tag{4}$$

At low to moderate air flow rates the data correspond to the single-phase prediction and correlate in terms of Re_G. This can be expected because large parts of the duct walls are dry during stratified flow and there is no significant interaction on the interface. As flooding is approached the pressure drop starts to rise due to the presence of vortices and the wavy interface. The same data are plotted in Fig. 5(b) against the densimetric gas Froude based on the duct height

$$Fr_{HG} = \frac{\rho_G V_G^2}{gH(\rho_L - \rho_G)}. \tag{5}$$

The choice of H for the characteristic dimension in the gas Froude number will be explained in detail in Section 4 on the flooding results. At this stage it is very important to note that the air flow rate at which the strong pressure rise occurs is not related to the gas Reynolds number but to the Froude number as defined in Eq. (5). It can be concluded that pressure gradient inside the ducts is related to Re_G at low to moderate gas flow rates and that Fr_{HG} becomes the governing parameter at higher gas flow rates at the onset of stronger phase interaction. In the region where the f_G–Re_G relationship holds the friction factor data does not correlate in terms of the gas Froude number, as can be seen in Fig. 5(b).

Note that the hydraulic diameter is taken as the required length dimension in the gas Reynolds number while the duct height is employed in the Froude number to obtain correlation at higher gas flow rates. This implies that the hydraulic diameter is the characteristic duct dimension at low to moderate gas flow rates and that the duct height becomes the characteristic dimension upon the onset of stronger phase interaction.

3.3.2. The effect of the fluid properties on the pressure drop characteristics

Friction factor data for air–methanol, helium–methanol and hydrogen–methanol flow in the 50 mm duct (W = 10 mm) are plotted in Fig. 6(a) and (b) against the gas Reynolds and Froude number respectively. Analogous to Fig. 5(a) and (b) the friction factor data correlate in terms of the gas Reynolds number at low to moderate gas flow rates while at higher gas flow rates the pressure drop is governed by the gas Froude number.

The results on the role of the dimensionless groups presented in Fig. 5 were obtained by varying the duct geometry while keeping the fluid properties constant. In Fig. 6 the duct geometry was kept the same and the fluid properties are varied. Both these independent methods confirm the fundamental role of the gas Reynolds and Froude number during gas–

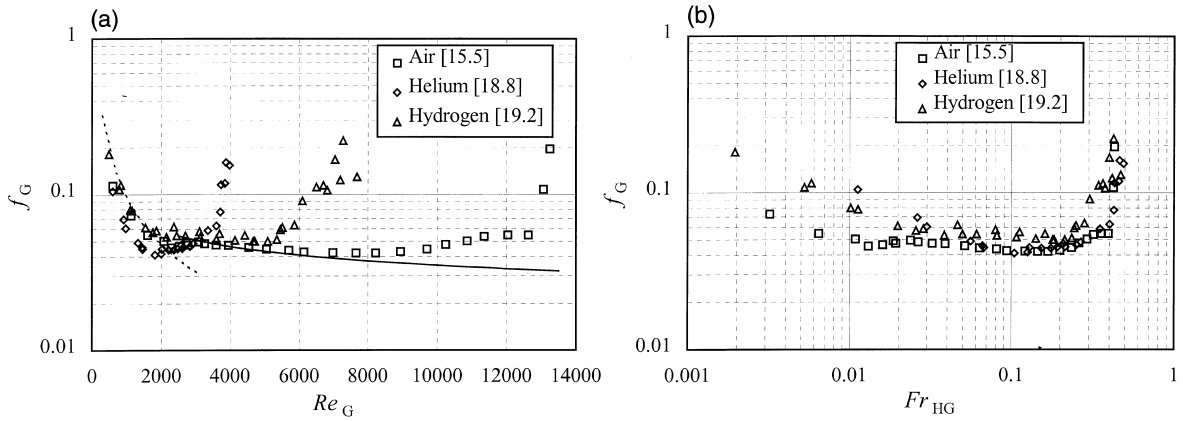

Fig. 6. (a) Two-phase friction factor measured for air–methanol, helium–methanol and hydrogen–methanol flow plotted against the gas Reynolds number. $H = 50$ mm, $W = 10$ mm, $\theta = 60°$. Broken and solid line: Laminar and turbulent single-phase friction factor. $[V_L]$, m/s $\times 10^3$. (b) Two-phase friction factor measured for air–methanol, helium–methanol and hydrogen–methanol flow plotted against the gas Froude number. $H = 50$ mm, $W = 10$ mm, $\theta = 60°$. $[V_L]$, m/s $\times 10^3$.

liquid counterflow. Figs. 5(a) and 6(a) in particular demonstrate that the gas Reynolds number and the duct hydraulic diameter do not determine when flooding occurs.

4. Experimental results: flooding

Consider Fig. 7(a) showing air–water flooding data for a duct inclination of 60° to the horizontal. The figure presents the air superficial velocity at flooding for the four rectangular ducts tested. It is evident from Fig. 7(a) that the flooding gas velocity is strongly dependent on

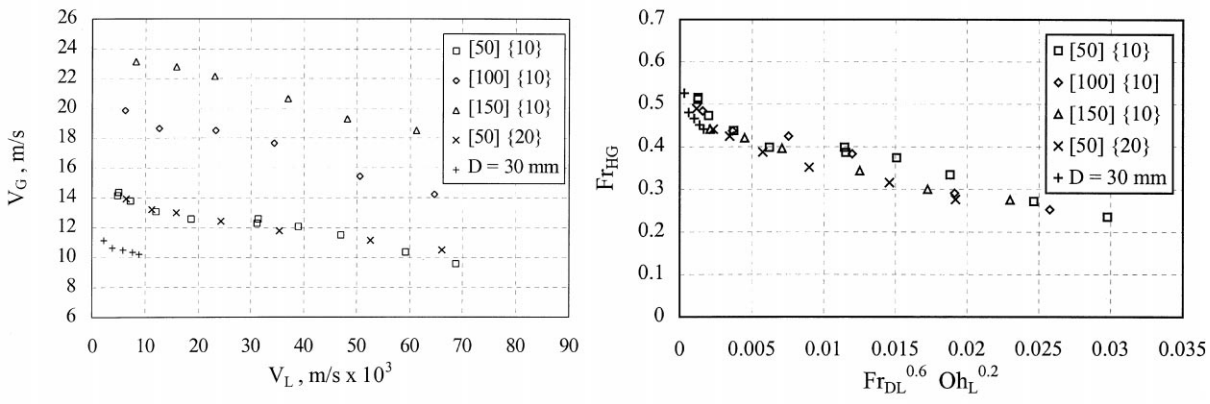

Fig. 7. (a) Air–water flooding superficial velocities for rectangular ducts inclined at 60° to the horizontal. $[H]$, mm; $\{W\}$,mm. The data for the $D = 30$ mm tube is taken from Zapke and Kröger (1996). (b) The data shown in Fig. 7(a) presented in a dimensionless form in terms of the densimetric Froude numbers and the Ohnesorge number.

the duct height, experiencing an increase as the duct height increases. The trend can be explained in terms of the mechanism by which flooding occurs: When the size of a liquid vortex has grown at the inlet of the duct to obstruct the flow path of the gas, it is propelled upwards and liquid travels up past the injection point to cause flooding. The weight of the liquid contained in the vortex is proportional to the duct height and the density difference between the two phases. This weight must be overcome by the drag force exerted by the gas flow which is proportional to the momentum flux $\rho_G V_G^2$. The densimetric gas Froude number based on the duct height, as defined by Eq. (5), is a ratio of these two forces which successfully correlates the observed height effect as illustrated in Fig. 7(b). The liquid Froude number

$$Fr_{DL} = \frac{\rho_L - V_L^2}{gD_e(\rho_L - \rho_G)} \tag{6}$$

on the abscissa is based on the hydraulic diameter. Using different characteristic dimensions for the gas Froude number (height) and the liquid Froude number (hydraulic diameter) follows from the empirical approach to correlate the data. Attempts to correlate the data in terms of phase Froude numbers containing the same characteristic dimension or making use of a ratio of the duct height and width failed.

The Ohnesorge number

$$Oh_L = \sqrt{\frac{\eta_L^2}{\rho_L D_e \sigma}} \tag{7}$$

forming part of the independent parameter on the abscissa is required to correlate the effect of the liquid properties on the flooding gas velocity. In part II the role of the Ohnesorge number is discussed in more detail. In Eq. (7) σ is the surface tension.

The duct height forming part of Fr_{HG} is critical to the correlation of the trend depicted in Fig. 7(a). Employing the hydraulic diameter in the gas Froude number fails to correlate this trend. The three ducts of 10 mm width have approximately equal hydraulic diameters and yet their flooding gas velocities differ significantly.

The Kutateladze number

$$Ku_G = \frac{\rho_G^{1/2} V_G}{\left[g\sigma(\rho_L - \rho_G)\right]^{1/4}} \tag{8}$$

frequently used in the literature to present flooding data also fails to correlate the predominant height effect. Ku_G is formed by substituting the length dimension in the Froude number with an equivalent characteristic dimension containing gravity, phase densities and surface tension. As a result the Kutateladze number does not contain a physical dimension and therefore cannot represent the physics of flooding observed in the present investigation.

Also shown in Fig. 7(a) and (b) are flooding data by Zapke and Kröger (1996) for air–water flow in a 30 mm i.d. tube with a square-edged gas inlet, inclined at 60° to the horizontal. In Fig. 7(b) the tube diameter is taken as the length dimension required in the gas Froude number. The correlation achieved is remarkable, implying that the height perceived by the vortex at flooding is the diameter. In other words the dimensionless groups given by Eqs. (5)

and (6) successfully describe the geometry effect for both rectangular ducts and tubes when the height and diameter respectively are taken as the characteristic length dimension in the gas Froude number.

Flooding data for air–water, air–methanol and air–propanol are shown in Fig. 8. The tests were conducted with the 50 mm duct ($W = 10$ mm) in the vertical position. The methanol and the propanol flood at lower gas velocities than water because of their lower densities. The fact that the propanol flooding gas velocities are lower than for methanol means that the flooding gas velocity decreases with an increase in the liquid viscosity. These two liquids have equal densities and surface tensions, while the propanol viscosity is approximately four times the viscosity of methanol. The difference in the gas flooding velocities for methanol and propanol is therefore purely a viscosity effect.

Air–water flooding data measured for various duct inclinations from close to the horizontal to the vertical are shown in Fig. 9. The flooding gas velocity increases with an increase in the duct inclination due to the increasing gravity component which has to be overcome in the direction of the gas flow. A maximum is reached in the range $60^\circ < \theta < 70^\circ$, where θ is the duct inclination to the horizontal. Above an inclination of 70° the flooding gas velocity decreases fairly sharply. The vertical ducts were found to flood at significantly lower velocities than for inclinations just off the vertical.

The effect of the duct height on the flooding gas velocity as depicted in Fig. 7(a) was observed for all the inclinations tested from close to the horizontal to 80°. In the case of counterflow in the vertical ducts elements of churn-type flow and vortices were observed as described in Section 3.2. Here the height effect was not as pronounced as for inclined flow most probably because the vortex size did not reach the entire duct height during the churning

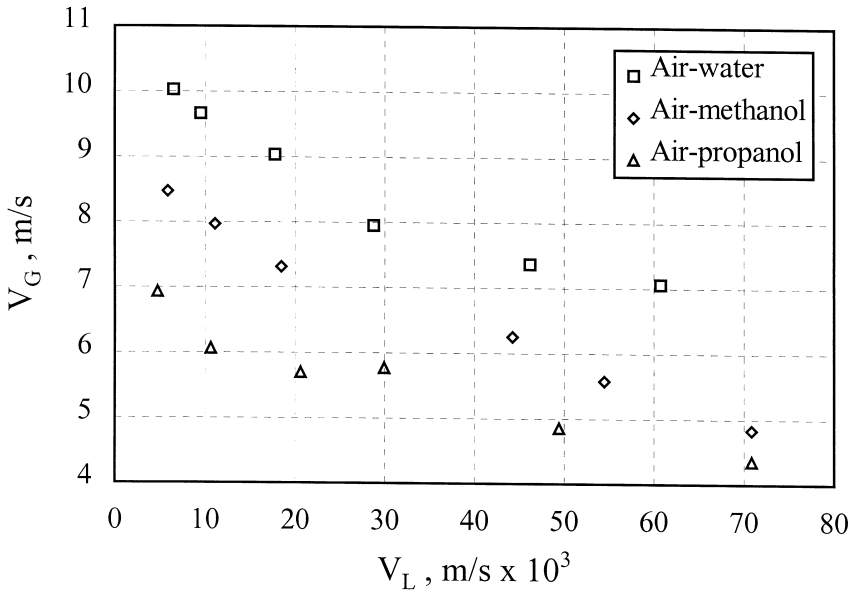

Fig. 8. Superficial velocities obtained with air–water, air–methanol and air–propanol to illustrate the effect of the liquid properties. $H = 50$ mm, $W = 10$ mm, $\theta = 90^\circ$.

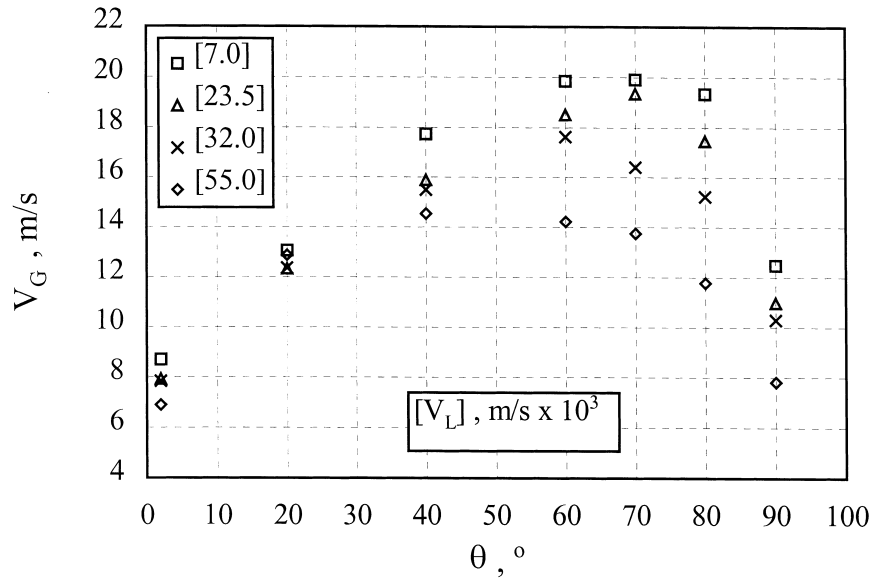

Fig. 9. Air–water flooding data measured with the 100 mm duct plotted against the duct inclination with the water flow rate as a parameter.

flow. The relatively smaller vortex size partly explains the significant decrease in the flooding gas velocity experienced for a change in inclination from $\theta = 80^\circ$ to 90°. A smaller vortex size implies the weight of the liquid contained in the vortex is less and thus a lower gas velocity is required for upward liquid transport. Furthermore the stabilising gravity component acting on the liquid film perpendicular to the duct axis vanishes as the inclination approaches the vertical. This contributes to the decrease in the flooding gas velocity.

5. Flooding correlations

The flooding data measured for vertical ducts is correlated by the relation

$$Fr_{\mathrm{HG}} = \frac{0.0055}{Fr_{\mathrm{DL}}^{0.2} Oh_{\mathrm{L}}^{0.3}}. \tag{9}$$

All the flooding data for vertical ducts are shown in Fig. 10 against the predicted values according to Eq. (9). The majority of the data lie in a $\pm 15\%$ band.

The data for flooding in inclined ducts were found to correlate in terms of an exponential function

$$Fr_{\mathrm{HG}} = K_0 \exp(-n Fr_{\mathrm{DL}}^{0.6} Oh_{\mathrm{L}}^{0.2}) \tag{10}$$

where K_0 and n are functions of the duct inclination:

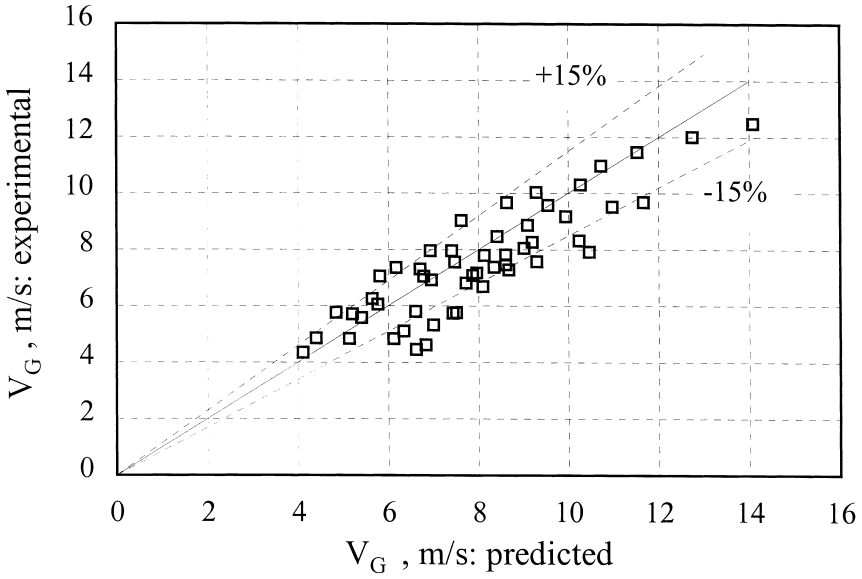

Fig. 10. Experimental versus the predicted flooding gas velocities according to Eq. (9) for counterflow in vertical ducts.

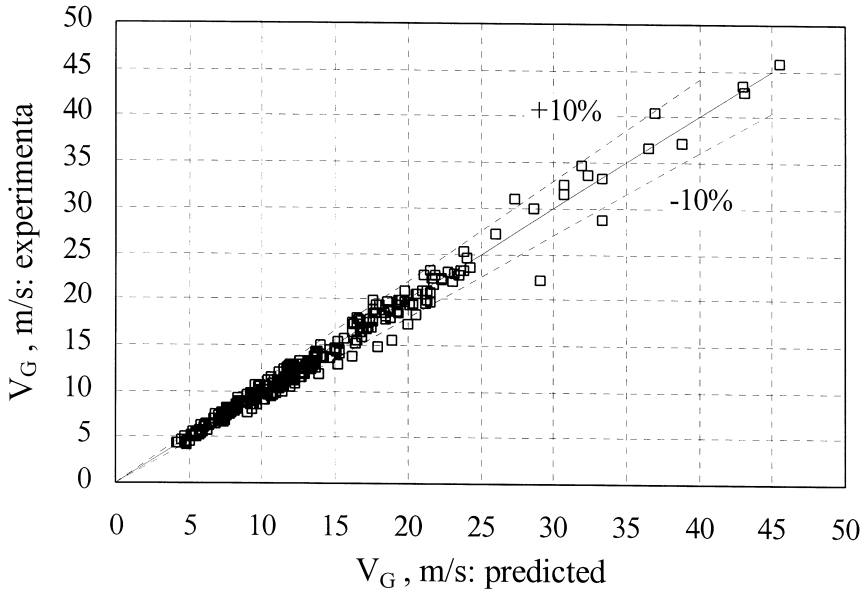

Fig. 11. Experimental versus the predicted flooding gas velocities according to Eq. (10) for counterflow in inclined ducts.

$$K_0 = 7.9143 \times 10^{-2} + 4.9705 \times 10^{-3}\theta + 1.5183 \times 10^{-4}\theta^2 - 1.9852 \times 10^{-6}\theta^3 \tag{11}$$

$$n = 1.8149 \times 10^{1} - 1.9471\theta + 6.7058 \times 10^{-2}\theta^2 - 5.3227 \times 10^{-4}\theta^3. \tag{12}$$

The flooding data measured for the inclined ducts as summarised in Table 2 are shown in Fig. 11 against the values predicted according to Eq. (10). The measured values vary from as low as 5 m/s to a maximum of $\approx$45 m/s as a result of the wide range of dimensions, duct inclinations and fluid properties tested. The superficial velocities cover almost an order of magnitude. According to Fig. 11 this wide range of velocities is correlated with an accuracy of $\pm$10%.

6. Conclusions

At low to moderate gas flow rates the flow inside inclined ducts is stratified and the pressure drop experienced by the gas is related to the gas Reynolds number. The length dimension required in the gas Reynolds number is the hydraulic diameter. At higher gas flow rates the pressure drop rises above the corresponding gas-only single-phase pressure drop and the densimetric gas Froude number becomes the governing parameter where the ducts height is the important dimension.

The flooding gas velocity in inclined ducts is proportional to the square root of the duct height. Such a strong height effect was not observed in vertical ducts.

The flooding gas velocities correlate in terms of the phase Froude numbers where the duct height and the hydraulic diameter were found to be the characteristic dimensions in the gas and liquid Froude number respectively. This is a new concept. In the past the hydraulic diameter has usually been employed for both phases.

As a result of the strong height effect the Kutateladze number fails to correlate the present flooding data.

Comparison of the present flooding data for rectangular ducts to data for tubes has revealed that the diameter is the effective height during gas–liquid counterflow in inclined tubes. Thus while the height is the important dimension for rectangular ducts, the diameter becomes the characteristic dimension in the case of tubes.

The role of the liquid viscosity and surface tension is secondary to that of the phase densities and the duct dimensions during flooding. The liquid viscosity was found to have a stronger effect than the surface tension.

The main mechanism of upward liquid transport during flooding in inclined ducts is the formation of a vortex-type flow pattern where liquid is propelled upwards in the form of a rotating gas–liquid mixture. The contribution by entrainment appears to be negligible.

References

Barnea, D., Yoseph, N., Taitel, Y., 1986. Flooding in inclined pipes — effect of entrance section. The Canadian Journal of Chemical Engineering 64, 177–184.

Chung, K.S., Liu, C.P., Tien, C.L., 1980. Flooding in two-phase countercurrent flows — II: Experimental investigation. PhysicoChemical Hydrodynamics 1, 209–220.

Clift, R., Pritchard, C., Nedderman, R.M., 1966. The effect of viscosity on the flooding conditions in wetted wall columns. Chemical Engineering Science 21, 87–95.

Feind, R., 1960. Falling liquid films with countercurrent air flow in vertical tubes. VDI Forschungsheft 481, 5–35.

Govan, A.H., Hewitt, G.R., Richter, H.J., Scott, A., 1991. Flooding and churn flow in vertical pipes. Int. J. Multiphase Flow 17, 27–44.

Hewitt, G.F., Hall-Taylor, N.S., 1970. Annular Two-Phase Flow. Pergamon Press, Oxford.

Lee, S.C., Bankoff, S.G., 1983. Stability of steam-water countercurrent flow in an inclined channel. Journal of Heat Transfer 105, 713–718.

Lee, S.C., Bankoff, S.G., 1984. Parametric effects on the onset of flooding in flat-plate geometries. International Journal of Heat Mass Transfer 27, 1691–1700.

Suzuki, S., Ueda, T., 1977. Behaviour of liquid films and flooding in counter-current two-phase flow — part 1. Flow in circular tubes. Int. J. Multiphase Flow 3, 517–532.

White, F.M., 1991. Viscous Fluid Flow, 2nd ed. McGraw-Hill, New York.

Whalley, P.B., McQuillan, K.W., 1985. Flooding in two-phase flow: the effect of tube length and artificial wave injection. PhysicoChemical Hydrodynamics 6, 3–21.

Zapke, A., Kröger, D.G., 1996. The influence of fluid properties and inlet geometry on flooding in vertical and inclined tubes. Int. J. Multiphase Flow 22, 461–472.